# Electronic Supplementary Information

*for*

# A p-π* Conjugated Triarylborane as an Alcohol-Processable n-Type Semiconductor for Organic Optoelectronic Devices

Yingjian Yu,†[ab] Changshuai Dong,†[ab] Abdullah F. Alahmadi,[c] Bin Meng,*[a] Jun Liu,*[a] Frieder Jäkle*[c] and Lixiang Wang[a]

**Table of Contents**

## 1. Characterization methods

**General.** $^{1}H$ NMR and $^{13}C$ NMR spectra were recorded on a Bruker AV-400 or AV-500 spectrometer. The $^{11}B$ NMR spectrum was acquired with a boron-free quartz NMR tube on a Bruker AV-500 equipped with a 5mm PH SEX 500S1 11B-H/F-D probe. Elemental analysis was performed with a Bio-Rad elemental analysis system. Gel permeation chromatography (GPC) was carried out at 35 $^{o}C$ with a Waters 410 instrument using tetrahydrofuran as the eluent and mono-disperse polystyrene as the standard. Thermal gravimetric analysis (TGA) was performed under an $N_2$ flow at a heating rate of 10 $^{o}C$/min with a Perkin-Elmer-TGA 7 system. The reported temperature of degradation ($T_d$) corresponds to a 5% weight loss. UV-vis absorption spectra were measured with a Shimadzu UV-3600 spectrometer. Cyclic voltammetry (CV) was performed on a CHI660a electrochemical analyzer system at a scan rate of 50 mV $s^{-1}$. The organic molecules were tested in 1 mM dichloromethane solutions with the ferrocene/ferrocenium couple as the reference. The supporting electrolyte was 0.1 M tetrabutylammonium hexafluorophosphate ($n$-$Bu_4NPF_6$). The HOMO and LUMO energy levels were estimated by the equations: $E_{HOMO}/E_{LUMO} = -e(4.80\ V + \phi_{ox}^{onset}/\phi_{red}^{onset})$, where $\phi_{ox}^{onset}/\phi_{red}^{onset}$ represents the onset potential of the oxidation/reduction waves. The thickness of pristine or blended films was measured with a Dektak 6M Stylus Profile. Atomic force microscopy (AFM) was performed with a SPA300HV (Seiko Instruments, Inc., Japan) in tapping mode. The geometry optimizations of **BDT** and **TT** were performed by DFT calculations using the Gaussian 09 program[1] at the B3LYP/6-31G* level of theory.

## 2. Materials and synthetic procedures

**Materials.** The di-stannylated monomer (2,4,6-tri-tert-butylphenyl)bis(5-(trimethylstannyl)thiophen-2-yl)borane (**4**) was synthesized according to our previous work,[2] the di-bromo monomer 1,4-dibromo-2,5-bis(1,3-bis(2-(2-(2-methoxyethoxy)ethoxy)-ethoxy)propan-2-yloxy)benzene (**M1**) and the di-stannylated monomer 4,7-bis(5-trimethylstannylthiophen-2-yl)-5,6-difluoro-2,1,3-benzothiadiazole (**M2**) were synthesized in our lab following the literature methods.[3] 2-bromo-3-(2-ethylhexyl)thiophene (**1**) and 2-(trimethylstannyl)-5-(5-(trimethylstannyl)thiophen-2-yl)thiophene (**5**) were purchased from Energy-Chemical Company. All other chemicals were purchased from the Beijing Chemical Plant, Aldrich, Alfa and used without further purification unless otherwise stated. Toluene, tetrahydrofuran and N,N-dimethylformamide were distilled before use.

**Synthesis of 5-bromo-4-(2-ethylhexyl)thiophene-2-carbaldehyde (2).** To a solution of 2-bromo-3-(2-ethylhexyl)thiophene (**1**) (1.20 g, 4.36 mmol) in anhydrous tetrahydrofuran (20 mL) at -78 °C was added dropwise a 2.0 M lithium diisopropylamide solution in tetrahydrofuran (2.18 mL, 4.36 mmol). After stirring at -78 °C for 2 hours, to the mixture was added dropwise N,N-dimethylformamide (1.01 g, 13.08 mmol), followed by stirring over night while allowing to warm to room temperature. After workup, the reaction mixture was poured into water, then extracted with ether three times. The combined organic phase was washed with brine, dried over anhydrous $Na_2SO_4$, filtered, and concentrated in vacuum. Finally, the residue was purified by silica gel column chromatography with petroleum ether/ethyl acetate = 10/1 as eluent to afford the title compound as a yellow oil (0.94 g, 71%). $^1$H NMR (400 MHz, $CDCl_3$), δ (ppm): 9.76 (s, 1H), 7.43 (s, 1H), 2.53 (d, *J* = 7.2 Hz, 2H), 1.62 (dd, *J* = 12.5, 6.5 Hz, 1H), 1.35 – 1.25 (m, 8H), 0.89 (dd, *J* = 9.4, 5.4 Hz, 6H). $^{13}$C NMR (126 MHz, $CDCl_3$), δ (ppm): 181.92, 143.18, 142.75, 137.29, 122.65, 39.89, 33.71, 32.42, 28.76, 22.99, 14.09, 10.77.

$^1$H NMR

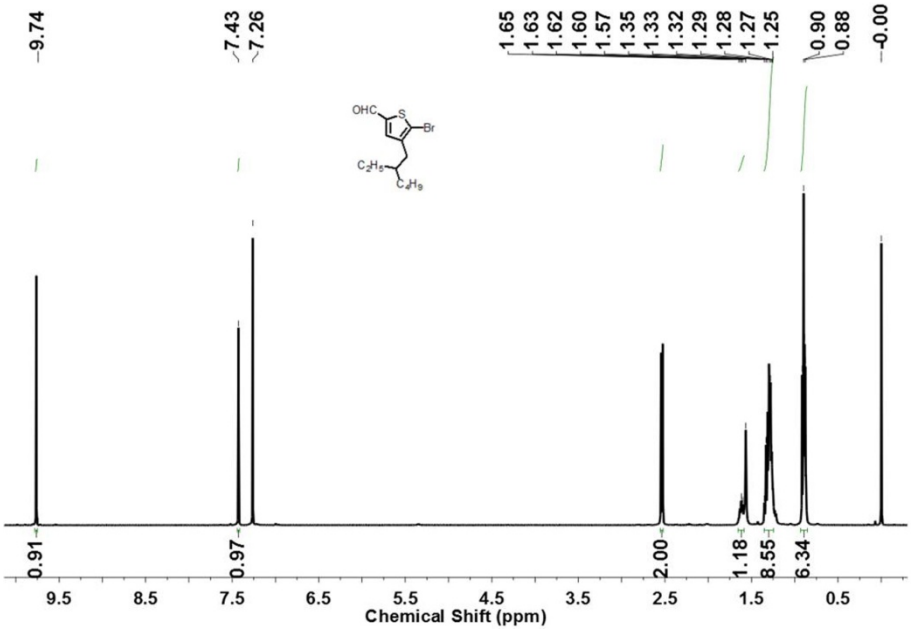


$^{13}$C NMR

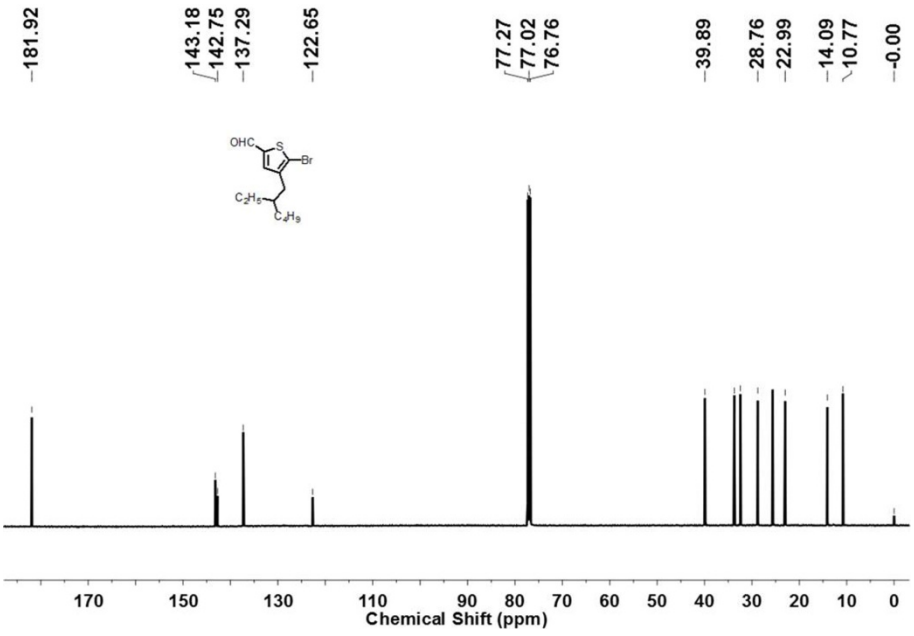

**Synthesis of 2-((Z)-5-((5-bromo-4-(2-ethylhexyl)thiophen-2-yl)methylene)-3-ethyl-4-oxothiazolidin-2-ylidene)malononitrile (3).** A mixture of 5-bromo-4-(2-ethylhexyl)thiophene-2-carbaldehyde (**2**) (0.26 g, 0.84 mmol), 2-(3-ethyl-4-oxothiazolidin-2-ylidene)malononitrile (0.33 g, 1.68 mmol) and anhydrous chloroform (35 mL) was stirred at room temperature under argon atmosphere. After adding three drops of piperidine, the mixture was warmed to reflux for 12 hours. After cooling to room temperature, the reaction mixture was concentrated in vacuum. The residue was purified by silica gel column chromatography with chloroform as eluent to afford the title compound as a yellow solid (0.38 g, 94%). $^1$H NMR (500 MHz, $CDCl_3$), δ (ppm): 7.94 (s, 1H), 7.12 (s, 1H), 4.31 (q, *J* = 7.2 Hz, 2H), 2.54 (d, *J* = 7.2 Hz, 2H), 1.65 – 1.58 (m, 1H), 1.40 (t, *J* = 7.2 Hz, 3H), 1.30 (dt, *J* = 20.6, 10.1 Hz, 8H), 0.92 – 0.86 (m, 6H). $^{13}$C NMR (126 MHz, $CDCl_3$), δ (ppm): 165.83, 165.25, 144.22, 136.28, 136.06, 128.02, 120.01, 114.58, 112.96, 112.16, 40.54, 39.90, 33.69, 32.21, 28.72, 25.63, 23.00, 14.18, 14.10, 10.77. Anal. Calcd. for $C_{21}H_{24}BrN_3OS_2$: C, 52.71; H, 5.06; N, 8.78; S, 13.40. Found: C, 52.46; H, 5.01; N, 8.69; S, 13.33.

$^1$H NMR

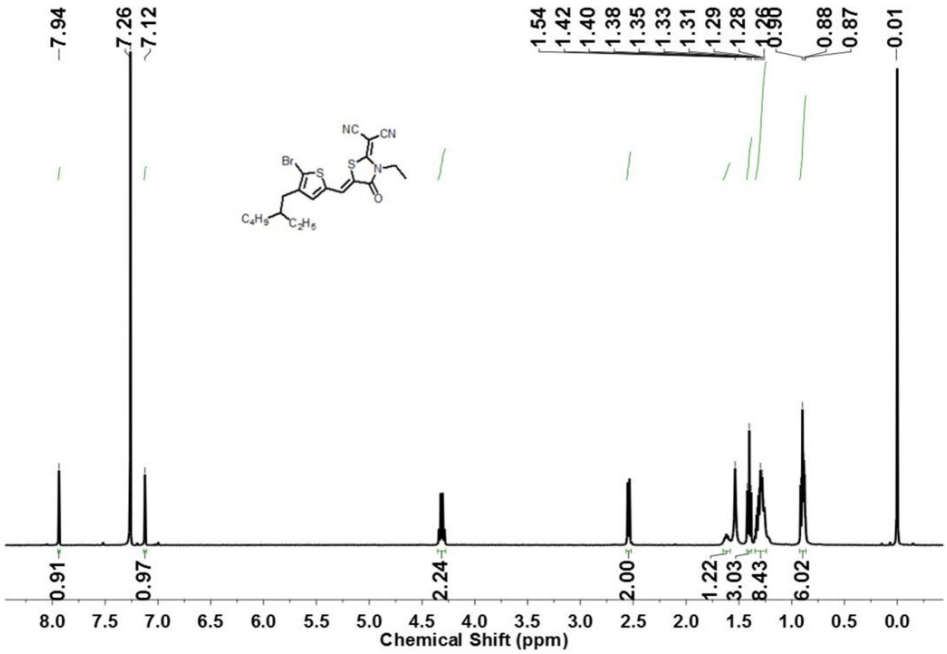


$^{13}$C NMR

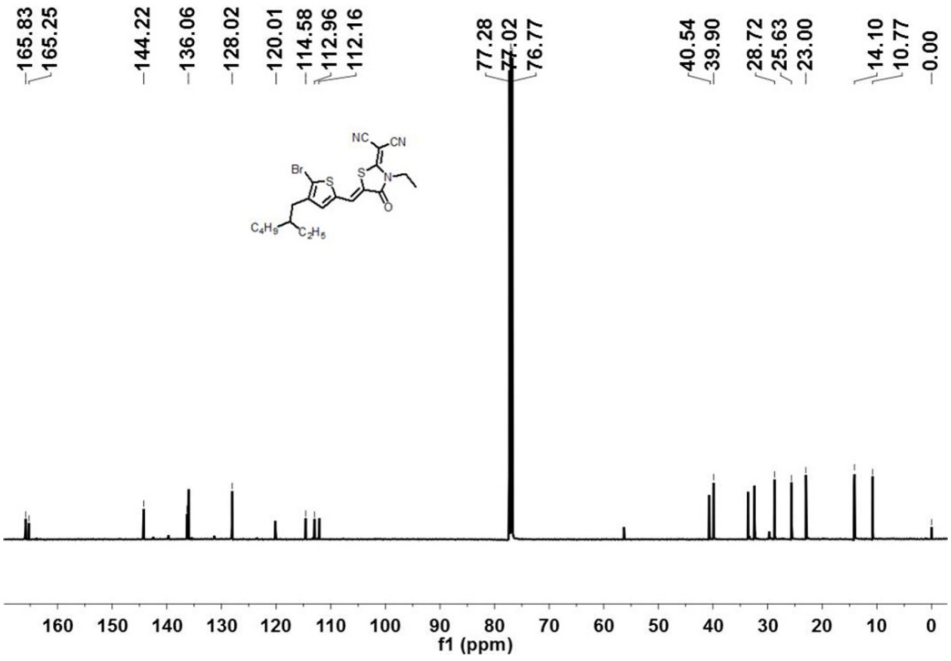

**Synthesis of BDT.** Under argon atmosphere, a mixture of 2-((Z)-5-((5-bromo-4-(2-ethylhexyl)thiophen-2-yl)methylene)-3-ethyl-4-oxothiazolidin-2-ylidene)malononitrile (**3**) (0.27 g, 0.57 mmol), (2,4,6-tri-tert-butylphenyl)bis(5-(trimethylstannyl)thiophen-2-yl)borane (**4**) (0.21 g, 0.28 mmol), $Pd(PPh_3)_4$ (13.2 mg, 0.010 mmol), CuI (3.3 mg, 0.020 mmol) and anhydrous toluene (15 mL) was stirred at 115 °C for 15 hours. After cooling to room temperature, the reaction mixture was concentrated in vacuum. The residue was purified by silica gel column chromatography with petroleum ether/ethyl acetate = 10/1 as eluent and then recrystallized in *n*-hexane/chloroform twice to afford the title compound as a red solid (0.10 g, 30%). $^1$H NMR (500 MHz, $CDCl_3$), δ (ppm): 8.01 (s, 2H), 7.73 (s, 2H), 7.46 (s, 2H), 7.42 (d, *J* = 3.7 Hz, 2H), 7.28 (s, 2H), 4.33 (q, *J* = 7.1 Hz, 4H), 2.80 (dt, *J* = 28.5, 10.8 Hz, 4H), 1.69 – 1.64 (m, 2H), 1.43 – 1.38 (m, 15H), 1.33 – 1.18 (m, 34H), 0.81 (t, *J* = 7.3 Hz, 12H). $^{13}$C NMR (126 MHz, $CDCl_3$), δ (ppm): 165.89, 165.46, 151.93, 150.04 (br, C-B), 149.11, 144.27, 141.78, 141.46 (br, C-B), 140.85, 139.19, 134.63, 129.34, 128.55, 122.82, 114.26, 113.14, 112.22, 40.69, 39.82, 38.69, 35.04, 34.74, 33.68, 32.24, 31.38, 28.48, 25.52, 22.99, 14.20, 14.07, 10.51. $^{11}$B NMR (160.4 MHz, $C_6D_6$), δ (ppm): 58.4 ($w_{1/2}$ = 3000 Hz). Anal. Calcd. for $C_{68}H_{81}BN_6O_2S_6$: C, 67.08; H, 6.71; N, 6.90; S, 15.80. Found: C, 66.97; H, 6.69; N, 6.71; S, 15.69.

$^1$H NMR

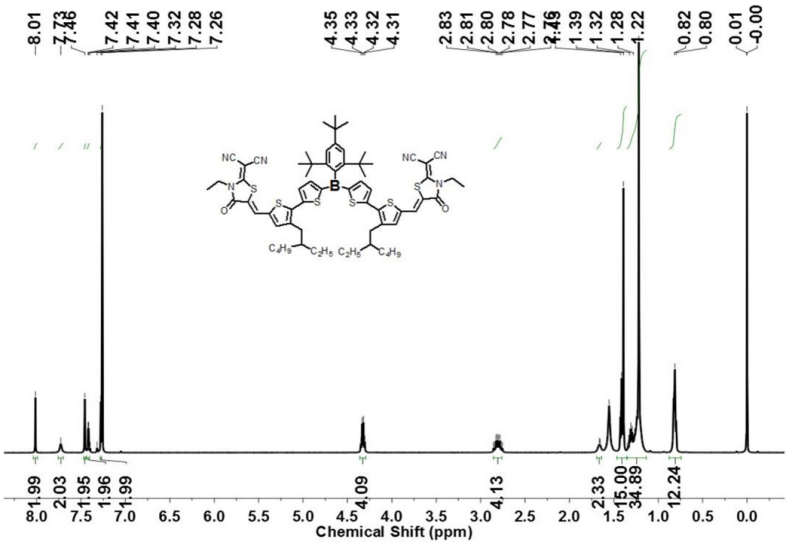


$^{13}$C NMR

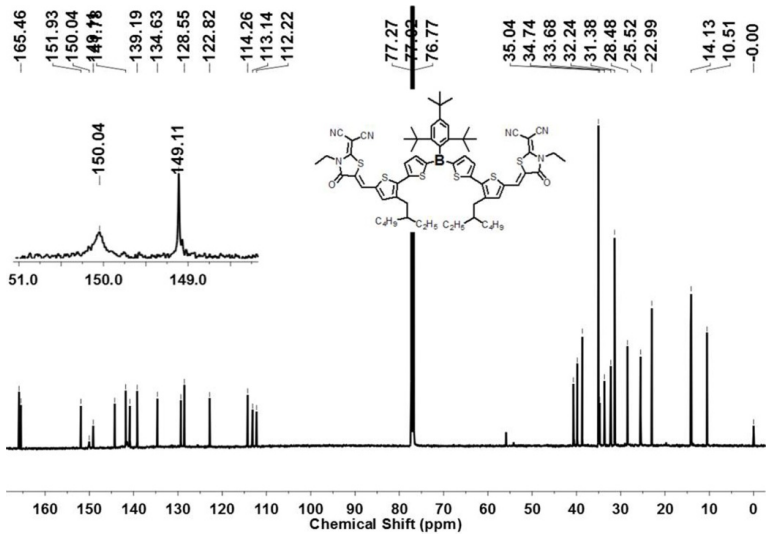


$^{11}$B NMR

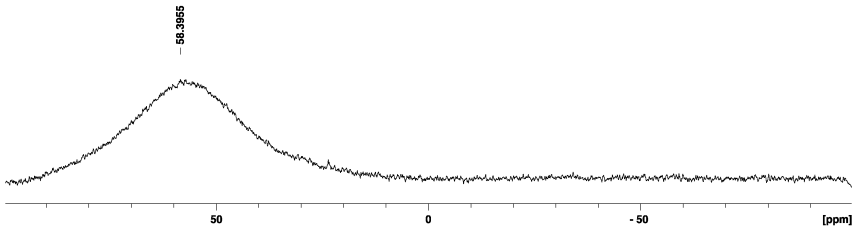

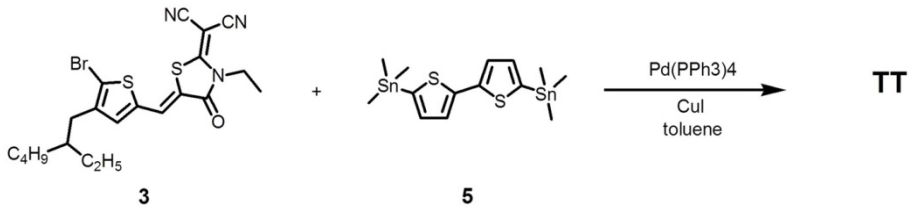


**Synthesis of TT.** Under argon atmosphere, a mixture of 2-((Z)-5-((5-bromo-4-(2-ethylhexyl)thiophen-2-yl)methylene)-3-ethyl-4-oxothiazolidin-2-ylidene)malononitrile (**3**) (0.14 g, 0.29 mmol), 2-(trimethylstannyl)-5-(5-(trimethylstannyl)thiophen-2-yl)thiophene (**5**) (0.070 g, 0.14 mmol), $Pd(PPh_3)_4$ (9.9 mg, 0.010 mmol), CuI (3.3 mg, 0.020 mmol) and anhydrous toluene (8 mL) was stirred at 115 °C for 15 hours. After cooling to room temperature, the reaction mixture was concentrated in vacuum. The residue was purified by silica gel column chromatography with chloroform/dichloromethane = 3/1 as eluent to afford the title compound as a dark-purple solid (0.12 g, 85%). $^1$H NMR (500 MHz, $C_6D_6$), δ (ppm): 7.78 (d, *J* = 5.4 Hz, 2H), 6.87 (d, *J* = 3.8 Hz, 2H), 6.84 (d, *J* = 3.9 Hz, 2H), 6.71 (d, *J* = 6.1 Hz, 2H), 3.66 (dd, *J* = 14.3, 7.1 Hz, 4H), 2.64 (t, *J* = 8.4 Hz, 4H), 1.62 (s, 2H), 1.26 (dd, *J* = 27.4, 16.4 Hz, 16H), 0.91 (d, *J* = 14.1 Hz, 12H), 0.84 (t, *J* = 7.4 Hz, 6H). $^{13}$C NMR (126 MHz, $CDCl_3$), δ (ppm): 165.88, 165.49, 140.98, 140.79, 139.17, 138.56, 134.15, 134.08, 128.68, 128.52, 124.82, 113.97, 113.38, 112.14, 40.86, 40.12, 33.88, 32.54, 28.69, 25.74, 23.04, 14.24, 14.21, 10.70. Anal. Calcd. for $C_{50}H_{52}N_6O_2S_6$: C, 62.47; H, 5.45; N, 8.74; S, 20.01. Found: C, 62.28; H, 5.40; N, 8.71; S, 19.87.

$^1$H NMR

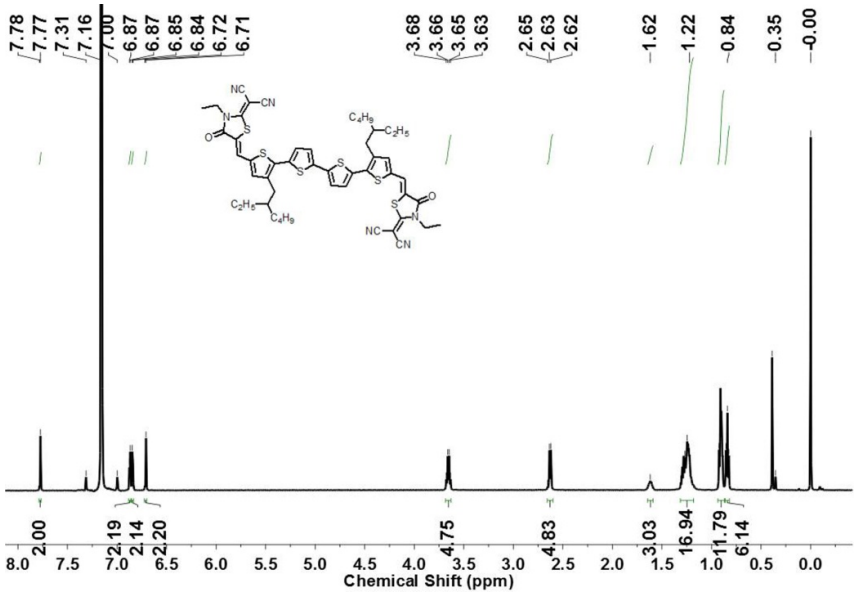


$^{13}$C NMR

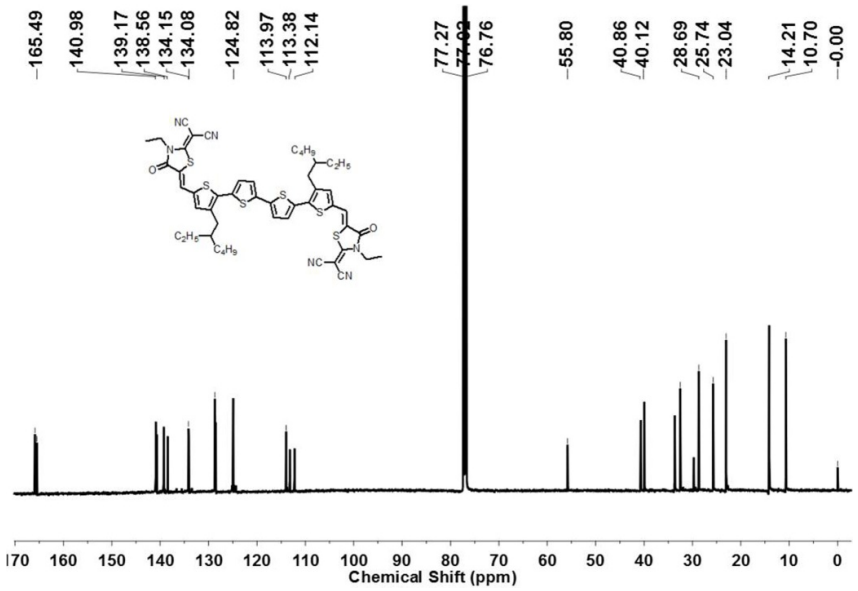

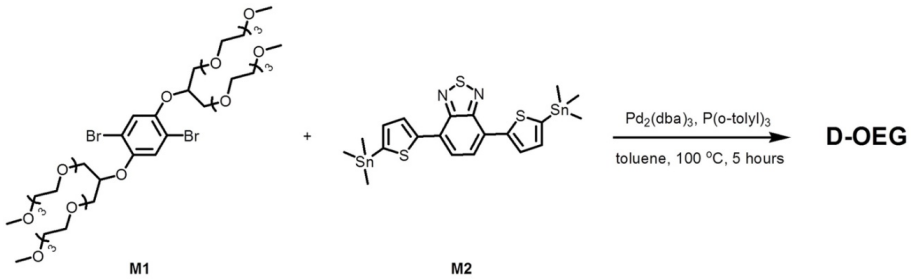


**Synthesis of D-OEG.** A mixture of di-stannylated monomer 4,7-bis(5-trimethylstannylthiophen-2-yl)-5,6-difluoro-2,1,3-benzothiadiazole (**M2**) (62.6 mg, 0.10 mmol), di-bromo monomer 1,4-dibromo-2,5-bis(1,3-bis(2-(2-(2-methoxyethoxy)ethoxy)-ethoxy)propan-2-yloxy)benzene (**M1**) (115.1 mg, 0.11 mmol), $Pd_2(dba)_3{\cdot}CHCl_3$ (1.8 mg, 0.0020 mmol), P(*o*-tolyl)$_3$ (2.4 mg, 0.0080 mmol) and degassed toluene (2.5 mL) was vigorously stirred at 100 °C under argon atmosphere for 5 hours. After cooling down, the resulting mixture was poured into *n*-hexane (50 mL) and the precipitate was collected by filtration. The crude polymer was washed in a Soxhlet apparatus first with *n*-hexane and then with chloroform (CF). The CF fraction was concentrated and poured into *n*-hexane. The polymer was recovered by filtration as a powder and dried in vacuum overnight. Yield: 0.10 g, 86%. $^1$H NMR (400 MHz, 1,2-dichlorobenzene-*d*4), δ (ppm): 8.45 (br, 2H), 8.13 (br, 2H), 8.08 (br, 2H), 8.00 (br, 2H), 5.07 – 4.99 (m, 2H), 4.19 (d, *J* = 4.8 Hz, 8H), 3.97 – 3.85 (m, 16H), 3.84 – 3.69 (m, 24H), 3.64 (t, *J* = 4.8 Hz, 8H), 3.45 (s, 12H). Anal. Calcd. for $C_{54}H_{78}N_2O_{18}S_3$: C, 56.92; H, 6.90; N, 2.46; S, 8.44. Found: C, 56.33; H, 7.05; N, 2.21; S, 8.01. GPC (THF, polystyrene standard, 35 °C), $M_n$ =23.8 kDa, PDI = 1.8.

$^1$H NMR

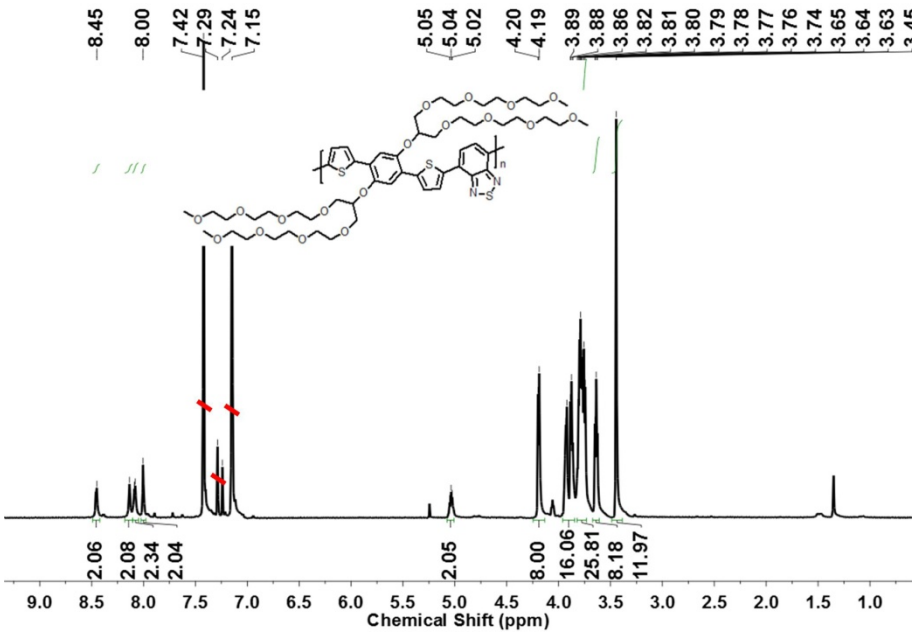

## 3. DFT calculations

The geometry optimizations, potential energy surface scan and natural dipole moment simulation by DFT methods of **BDT** and **TT** were performed using the Gaussian 09 program[1] at the B3LYP/6-31G* level of theory.

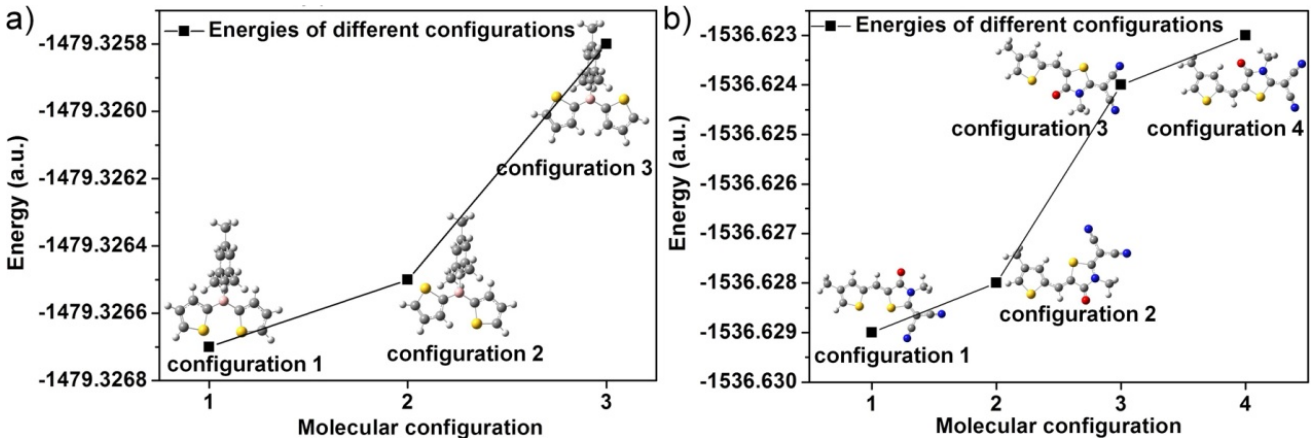


**Figure S1.** DFT calculation on the possible conformational isomers of molecular models of a) the triarylborane unit, b) the thiophene-linked terminal group.

The lowest energy conformations of the triarylborane unit and the thiophene-linked terminal group were determined to correctly present the chemical structure of **BDT**. The optimized geometry of the triarylborane unit with the lowest energy is the one for which the two sulfur atoms of the thiophene units adopt the same orientation and point away from the Mes* group (Figure S1a), leading to an axisymmetric structure. The optimized conformation of the thiophene-linked terminal group is the one for which the double bond between the thiophene unit and the terminal group adopts a "*Z*" geometry with the sulfur atoms oriented on the same side (Figure S1b).

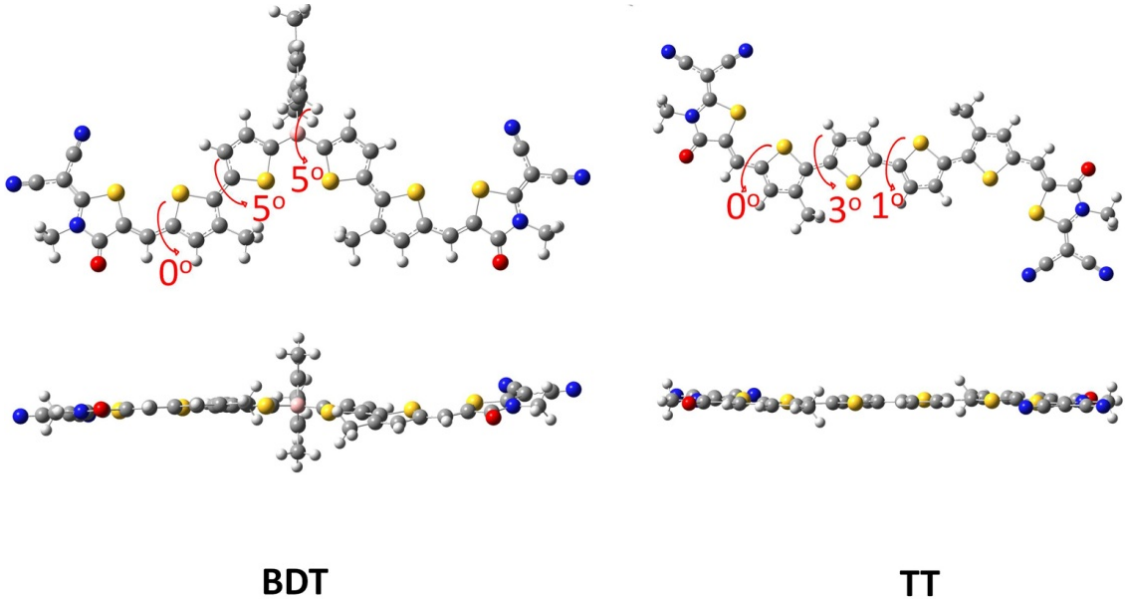


**Figure S2**. The optimized geometries of **BDT** and **TT** in top views (above) and side views (below).

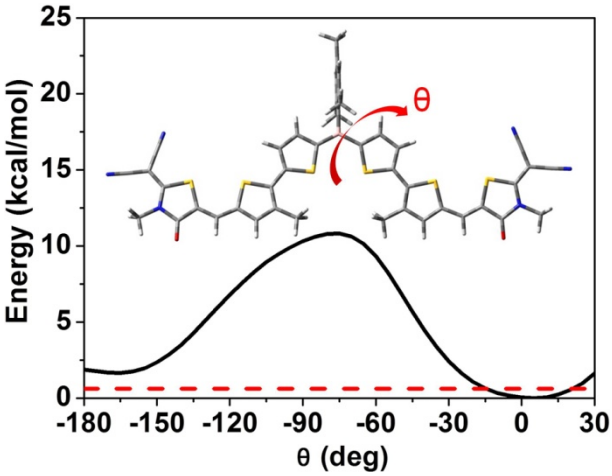


**Figure S3.** Potential energy surface scan of **BDT** calculated at the DFT B3LYP/6-31G* level for dihedral angles ($\vartheta$) between the two thienyls of triarylborane unit ranging from -180° to 30°. The red dashed line denotes $k_BT \approx 0.6$ kcal mol$^{-1}$ at 298 K.

DFT calculations reveal a broad and flat potential energy profile at around $\vartheta \approx 0°$, with an absolute minimum at 5°, which agrees well with the results of the geometry optimization. As the thermal fluctuations amount to about 0.6 kcal mol$^{-1}$ at 298 K, the potential energy profile is essentially flat for quasi-planar conformations ($\vartheta$: -15° to 21°), implying they are populated at room temperature. The results suggest that **BDT** possesses a great conformational freedom at its quasi-planar conformation with $\vartheta \approx 0°$, and further imply that the p-π* conjugated backbone with the boron atom is very flexible.

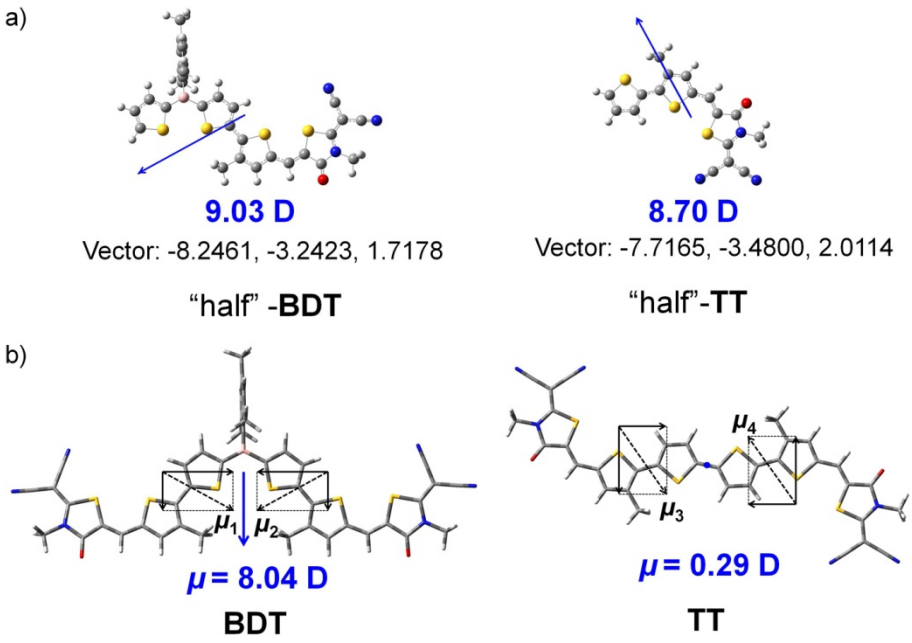


**Figure S4.** A) Theoretical simulation of the natural dipole moments of "half molecule" models of **BDT** and **TT**. b) Illustration of the overall natural dipole moment of **BDT** and **TT** via vector addition.

We evaluated the natural dipole moment ($\mu$) of **BDT**. The two non-collinear dipole moments, $\mu_1$ and $\mu_2$, obtained from the half molecule model of **BDT** (Figure S4a), give an overall $\mu$ as large as 8.04 Debye through vector addition. **TT** without the boron atom adopts a centrosymmetric structure with two end groups on opposite sides. As the result, the $\mu$ of **TT** is only 0.29 Debye due to two collinear dipole moments with almost opposite direction ($\mu_3$ and $\mu_4$). The small natural dipole moment of **TT** may be caused by its slightly twisted backbone configuration.

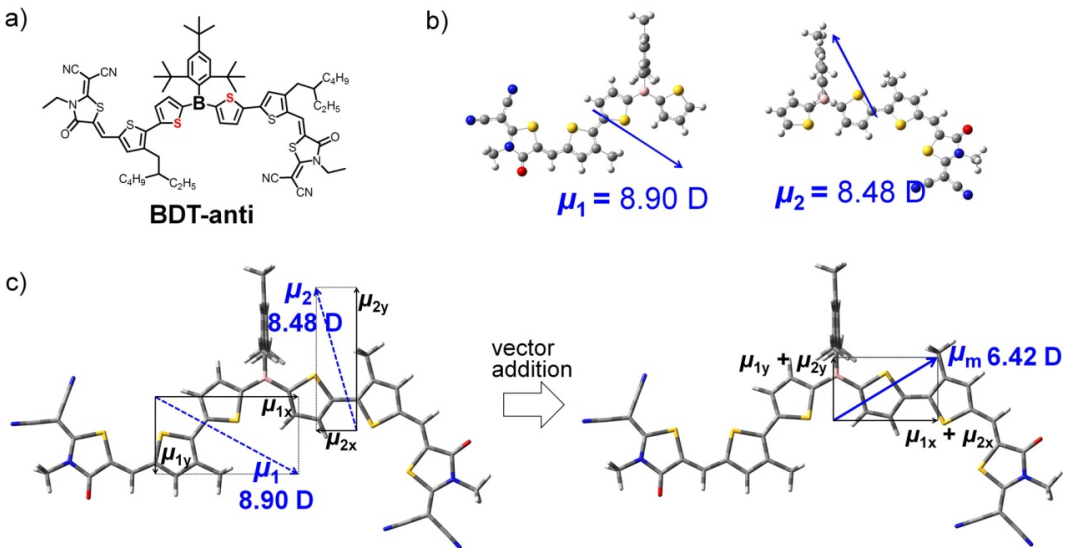


**Figure S5.** a) Chemical structure of **BDT-anti**. b) Theoretical simulation of the natural dipole moment of half molecule models of **BDT-anti**. c) The optimized geometry and illustration of the natural dipole moment of **BDT-anti** through vector addition.

Although an axisymmetric structure of **BDT** is preferred according to the DFT calculation (Figure S1, S2, S3), it should be pointed out that the two sulfur atoms of the thiophene units connected to boron may also adopt a trans orientation with one pointing toward and the other pointing away from the Mes* group, resulting in **BDT-anti** with a non-symmetric structure (Figure S5a). The calculated natural dipole moment ($\mu_m$) of **BDT-anti** is 6.42 Debye through vector addition of $\mu_1$ and $\mu_2$ obtained from the half molecule models (Figure S5b, c). The dipole moment is still much larger compared to that of the control molecule **TT**.

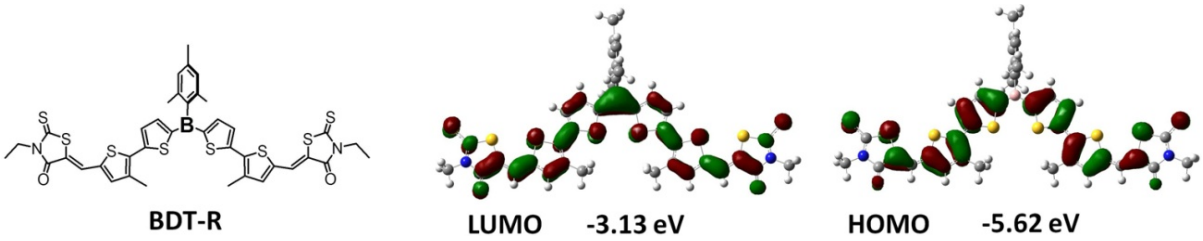


**Figure S6.** The Kohn–Sham LUMO/HOMO and $E_{LUMO}$/$E_{HOMO}$ of **BDT-R** based on DFT calculation.

To illustrate the influence of the terminal cyano groups (CN) of **BDT** on the spatial distribution and energy of the LUMO/HOMO, we performed calculations on the analogue **BDT-R** without CN groups for comparison. Although the calculated HOMO-LUMO gap of **BDT-R** is very similar to that of **BDT**, the LUMO/HOMO energy levels of **BDT-R** are much higher than those of **BDT** by 0.25/0.24 eV. These results confirm the pronounced effect of the strongly electron-withdrawing CN groups on the LUMO/HOMO energy.

**Table S1.** Coordinates (Å) for the optimized structure of **BDT**.

| Atom | x | y | z | Atom | x | y | z |
|---|---|---|---|---|---|---|---|
| S | 2.718897 | 3.775536 | 0.485816 | C | 5.795519 | 10.821218 | -0.355335 |
| C | 3.818194 | 2.410859 | 0.579969 | C | 6.065931 | 12.248294 | -0.520695 |
| C | 5.123681 | 2.894149 | 0.572885 | O | 5.257194 | 13.162687 | -0.471558 |
| C | 5.242126 | 4.291838 | 0.496188 | H | 5.054816 | -0.399540 | 4.159633 |
| B | 3.421674 | 0.917361 | 0.661093 | H | 4.721238 | 1.126866 | 3.332399 |
| C | 1.978552 | 0.358374 | 0.667509 | H | 3.492773 | -0.133130 | 3.374966 |
| S | 0.498923 | 1.296363 | 0.573187 | H | 4.743929 | 0.777702 | -1.964611 |
| C | -0.526196 | -0.122016 | 0.643292 | H | 3.568975 | -0.531670 | -1.901803 |
| C | 0.264757 | -1.263217 | 0.735643 | H | 5.171507 | -0.819463 | -2.591002 |
| C | 1.642447 | -0.990064 | 0.748438 | H | 8.444097 | -2.907788 | 1.860969 |
| H | 5.973426 | 2.223720 | 0.628995 | H | 7.396681 | -4.083296 | 1.066320 |
| H | 6.191959 | 4.814264 | 0.492638 | H | 8.446534 | -3.050424 | 0.095577 |
| H | -0.148024 | -2.264296 | 0.786480 | C | 1.249236 | 6.581499 | 0.726954 |
| H | 2.404733 | -1.757698 | 0.813276 | H | 0.878904 | 5.976503 | -0.108200 |
| C | 4.601948 | -0.139617 | 0.746316 | H | 1.228679 | 5.947691 | 1.619416 |
| C | 5.154310 | -0.700317 | -0.427958 | H | 0.543329 | 7.401595 | 0.880534 |
| C | 5.122623 | -0.538689 | 1.998709 | C | -2.427165 | 2.452355 | 0.226844 |
| C | 6.193353 | -1.632385 | -0.333476 | H | -1.890298 | 2.854377 | 1.093067 |
| C | 6.161186 | -1.473989 | 2.055887 | H | -1.771301 | 2.567363 | -0.642564 |
| C | 6.710093 | -2.036851 | 0.900345 | H | -3.310355 | 3.075306 | 0.064661 |
| H | 6.609348 | -2.052139 | -1.247250 | N | 7.443505 | 12.469461 | -0.758225 |
| H | 6.551770 | -1.768931 | 3.027862 | N | -7.698779 | -4.372880 | 1.144988 |
| C | 7.809100 | -3.069651 | 0.984680 | S | 7.298831 | 9.888458 | -0.511583 |
| C | 4.570975 | 0.041942 | 3.284169 | S | -5.137893 | -3.941987 | 1.137628 |
| C | 4.634786 | -0.299444 | -1.792908 | C | 7.912318 | 13.845044 | -0.955573 |
| C | -1.970255 | -0.070051 | 0.615594 | H | 8.367505 | 13.956715 | -1.940361 |
| C | -2.832607 | 1.018488 | 0.436678 | H | 7.031070 | 14.480341 | -0.877584 |
| S | -2.854912 | -1.569932 | 0.828709 | H | 8.637842 | 14.116804 | -0.187917 |
| C | -4.179223 | 0.614076 | 0.469106 | C | -9.026179 | -4.993624 | 1.205489 |
| C | -4.394758 | -0.747363 | 0.669517 | H | -9.744916 | -4.187301 | 1.065837 |
| H | -5.003415 | 1.309301 | 0.344682 | H | -9.138492 | -5.735514 | 0.413965 |
| C | 4.017260 | 4.949283 | 0.440041 | H | -9.182763 | -5.470308 | 2.173840 |
| C | 3.803946 | 6.375231 | 0.337606 | C | 8.237064 | 11.355783 | -0.786162 |
| C | 2.626972 | 7.123762 | 0.456868 | C | 9.604983 | 11.276463 | -0.993900 |
| S | 5.194379 | 7.396445 | 0.022838 | C | 10.216082 | 9.987039 | -0.979991 |
| C | 2.879119 | 8.498877 | 0.302133 | C | 10.468549 | 12.386050 | -1.222770 |
| C | 4.207278 | 8.844619 | 0.063292 | N | 11.211512 | 13.263503 | -1.412789 |
| H | 2.097712 | 9.249385 | 0.367228 | N | 10.693806 | 8.924311 | -0.964597 |
| C | -5.715487 | -1.290473 | 0.722534 | C | -6.511223 | -5.039670 | 1.272353 |
| H | -6.468060 | -0.514192 | 0.587005 | C | -6.300079 | -6.393302 | 1.481612 |
| C | 4.600647 | 10.206818 | -0.115678 | C | -7.323642 | -7.375825 | 1.609032 |
| H | 3.746009 | 10.878664 | -0.041010 | C | -4.954819 | -6.858864 | 1.580484 |
| C | -6.213279 | -2.548315 | 0.903197 | N | -8.127410 | -8.212405 | 1.719112 |
| C | -7.610695 | -2.975741 | 0.936831 | N | -3.848286 | -7.215917 | 1.657627 |
| O | -8.600417 | -2.271125 | 0.808138 | | | | |

**Table S2.** Coordinates (Å) for the optimized structure of **TT**.

| Atom | x | y | z | Atom | x | y | z |
|---|---|---|---|---|---|---|---|
| S | 5.487022 | 0.570847 | -0.285713 | H | 9.559836 | 0.700812 | -1.445434 |
| C | 3.193855 | 1.546144 | -0.958902 | C | -1.697015 | -0.719392 | 1.721183 |
| C | 4.153651 | 2.304465 | -1.655949 | H | -1.168848 | 0.175930 | 2.065112 |
| C | 3.066971 | -0.406878 | 0.675879 | H | -1.579645 | -0.771623 | 0.632836 |
| S | 1.317307 | -0.441468 | 0.778458 | H | -2.760334 | -0.579588 | 1.929623 |
| C | 1.340159 | -1.779639 | 1.922932 | N | 7.964021 | 8.251039 | -5.701364 |
| C | 2.651998 | -2.148043 | 2.180988 | N | -1.151286 | -8.124655 | 6.190577 |
| C | 3.612240 | -1.386104 | 1.488429 | S | 6.396014 | 6.605566 | -4.426390 |
| H | 2.126675 | 1.717172 | -1.041851 | S | 0.415729 | -6.470495 | 4.925650 |
| H | 3.893366 | 3.112346 | -2.330147 | C | 8.506710 | 9.369485 | -6.479560 |
| H | 2.912354 | -2.946085 | 2.866777 | H | 8.310694 | 10.317352 | -5.976860 |
| H | 4.680120 | -1.543440 | 1.587915 | H | 9.580284 | 9.197400 | -6.546853 |
| C | 0.142694 | -2.381822 | 2.456355 | H | 8.068174 | 9.391105 | -7.477990 |
| C | -1.192338 | -1.964916 | 2.399936 | C | -1.692688 | -9.245927 | 6.965600 |
| S | 0.286268 | -3.885475 | 3.343423 | H | -2.767536 | -9.079508 | 7.026493 |
| C | -2.057843 | -2.851530 | 3.077518 | H | -1.488706 | -10.192770 | 6.464140 |
| C | -1.437947 | -3.949183 | 3.657689 | H | -1.259954 | -9.265189 | 7.966601 |
| H | -3.123772 | -2.667228 | 3.137776 | C | 6.649601 | 8.079214 | -5.378150 |
| C | 5.464671 | 1.920756 | -1.416474 | C | 5.566993 | 8.882302 | -5.694942 |
| C | 6.661799 | 2.515557 | -1.958721 | C | 4.273906 | 8.488363 | -5.236466 |
| C | 7.994786 | 2.090859 | -1.911467 | C | 5.632401 | 10.087904 | -6.451941 |
| S | 6.521028 | 4.019746 | -2.845481 | N | 5.638514 | 11.078106 | -7.066021 |
| C | 8.860878 | 2.972497 | -2.594730 | N | 3.228281 | 8.147452 | -4.851591 |
| C | 8.243540 | 4.073749 | -3.170741 | C | 0.164214 | -7.945528 | 5.875810 |
| H | 9.925331 | 2.782142 | -2.661828 | C | 1.249208 | -8.742600 | 6.199561 |
| C | -1.307322 | -6.101842 | 4.964524 | C | 1.185601 | -9.948701 | 6.955917 |
| C | -2.045056 | -7.130775 | 5.714606 | C | 2.543019 | -8.341405 | 5.749493 |
| O | -3.244001 | -7.165149 | 5.921322 | N | 1.180997 | -10.939070 | 7.569742 |
| C | 8.116667 | 6.227227 | -4.476531 | N | 3.589179 | -7.994620 | 5.371380 |
| C | 8.855280 | 7.252109 | -5.231274 | C | 8.766387 | 5.164785 | -3.929811 |
| O | 10.053035 | 7.279816 | -5.445740 | H | 9.838810 | 5.175067 | -4.116546 |
| C | 8.497016 | 0.842654 | -1.235863 | C | -1.959483 | -5.043180 | 4.413418 |
| H | 8.380456 | 0.892650 | -0.147345 | H | -3.033033 | -5.059607 | 4.593107 |
| H | 7.966649 | -0.050754 | -1.581527 | C | 3.738557 | 0.554295 | -0.161436 |

## 4. Solubility characteristics

**Table S3.** The solubility of **BDT** and **TT** in various solvents.

| Solvent | **BDT** | **TT** |
|---|---|---|
| ethanol[a] | 1 mg/mL | < 0.1 mg/mL |
| 1-propanol[a] | 4 mg/mL | < 0.1 mg/mL |
| 1-butanol[a] | 7 mg/mL | < 0.1 mg/mL |
| 1-hexanol[a] | 9 mg/mL | < 0.1 mg/mL |

[a] The solubility is tested at 70 °C in various solvents.

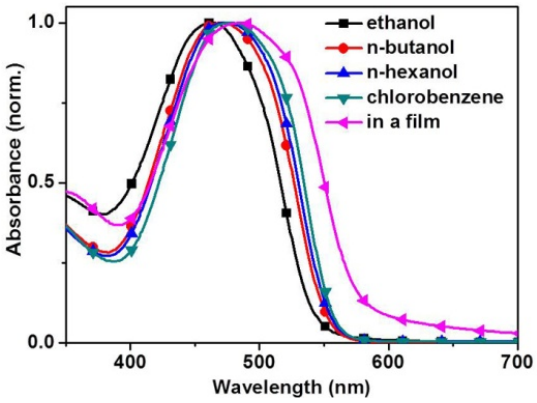


**Figure S7**. UV/vis absorption spectra of **BDT** in various solvents and in a film.

We tested the solubility of **BDT** and **TT** in various organic solvents. Both **BDT** and **TT** are well soluble in common halogenated solvents and aromatic solvents, such as chloroform, chlorobenzene, toluene, and xylene. **BDT** can also be dissolved in some alcohol solvents, such as ethanol, 1-propanol, 1-butanol and 1-hexanol. In contrast, **TT** can barely be dissolved at all in the aforementioned alcohol solvents with a solubility of less than 0.1 mg/mL. To further confirm the alcohol solubility of **BDT**, we measured its absorption spectra in various solvents and in a film. As shown in Figure S7, the absorption spectra in various alcohol solvents are quite similar to that in chlorobenzene. All the absorptions maxima are blue-shifted by 10-20 nm compared to data for a film, implying that **BDT** is well dissolved in all the solvents rather than dispersed in them.

## 5. Thermal properties and X-ray diffraction analyses

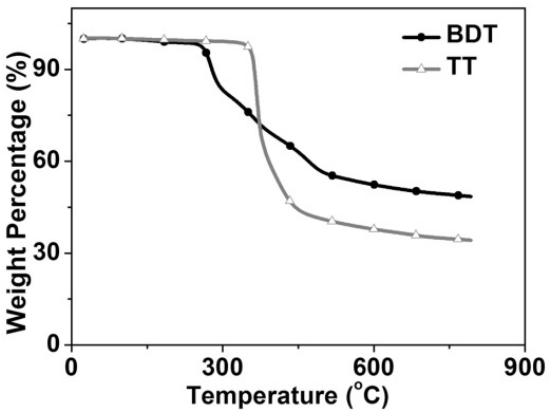


**Figure S8**. Thermogravimetric analysis (TGA) of **BDT** and **TT**.

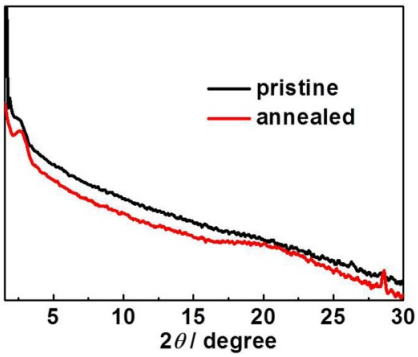


**Figure S9**. X-ray diffraction (XRD) patterns of **BDT** with and without thermal annealing at 120 °C.

The thermal properties of **BDT** and **TT** were determined by thermal gravimetric analysis (TGA) under $N_2$ flow. Both molecules exhibit good stability with thermal degradation temperatures ($T_d$) at 5% weight loss of 269 °C for **BDT** and 350 °C for **TT**. The possibility of π-stacking of **BDT** thin films was investigated via X-ray diffraction (XRD). The absence of obvious reflection peaks in the XRD patterns suggests that thin films of **BDT** are amorphous.

## 6. Fabrication of electron-only devices and electron mobility measurements

The electron-only device structure for the pristine films of **BDT** and **TT** was ITO/polyethyleneimine ethoxylated (PEIE)/**BDT** or **TT**/Ca/Al. The current-voltage curves in the dark were recorded with a Keithley 2400 source meter in the range of 0-8 V, and the results were fitted to a space-charge limited current (SCLC) equation, $J = (9/8)\,\varepsilon_0\varepsilon_r\mu\,(V^2/d^3)\exp[0.89\,\beta\,(V/d)^{1/2}]$, where $J$ is the current density at the space-charge limited region, d is the thickness of the active layer, μ is the zero field mobility, $\varepsilon_r$ is the relative dielectric constant of the blend (assumed to be 3.5), $\varepsilon_0$ is the permittivity of the free space ($8.85 \times 10^{-12}$ F $m^{-1}$), β is the field activation factor, and V is the potential across the device ($V = V_{applied} - V_{bias} - V_{series}$). $V_{series}$ represents the series and contact resistance of the device (10-15 Ω), which were measured using a blank device of ITO/PEDOT:PSS/$MoO_3$/Ag or ITO/PEIE/ Ca/Al.

## 7. Characterization of D-OEG

The synthesis of **D-OEG** is illustrated in the "Materials and synthetic procedures" section. Due to the long and branched OEG side chains, **D-OEG** is well soluble in alcohol solvents, such as 1-butanol and 1-hexanol. We estimated the $E_{LUMO}/E_{HOMO}$ of **D-OEG** from CV measurements, and measured the absorption spectra of **D-OEG** using UV-vis spectroscopy. The $E_{LUMO}/E_{HOMO}$ of **D-OEG** is estimated to be -3.39/-4.92 eV, which is matched well with the $E_{LUMO}/E_{HOMO}$ of **BDT**. The absorption spectrum of a film of **D-OEG** casted from its 1-hexanol solution peaks at 580 nm, which is also matched well with that of **BDT**.

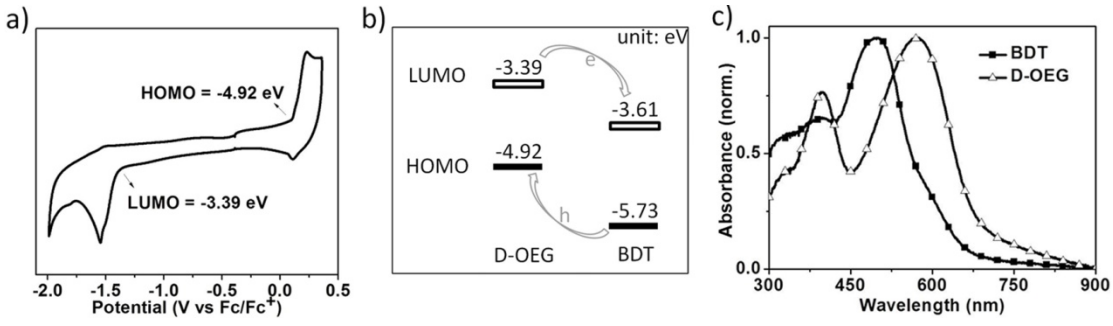


**Figure S10**. a) CV curves of **D-OEG**. b) Energy alignment of **D-OEG** and **BDT**. c) UV-vis absorption spectra of thin films of **BDT** and **D-OEG** casted from their 1-hexanol solution.

## 8. Alcohol-processing OSC devices fabrication and measurements

Indium tin oxide (ITO) glass substrates were cleaned successively with detergent, deionized water, acetone and isopropyl alcohol in an ultrasonic bath for 10 minutes each, followed by drying at 120 °C for 30 minutes and treatment with UV-ozone for 25 minutes. PEDOT:PSS (Baytron P Al 4083) was then spin-coated on the ITO glass substrates at 5000 rpm for 40 seconds and baked at 125 °C for 30 minutes to give a thickness of 40 nm. The active layer was spin-coated on top of the PEDOT:PSS layer using a solution of **D-OEG** (8 mg/mL) and **BDT** (8 mg/mL) in 1-butanol or 1-hexanol. Finally, the device was transferred to a vacuum chamber and Ca (20 nm)/Al (100 nm) was sequentially deposited by thermal evaporation at a pressure of about $2 \times 10^{-4}$ Pa. The active area of each device was 8 $mm^2$. The current density-voltage (*J*-V) characteristics of OSC devices were measured using a computer-controlled Keithley 2400 source meter and an Oriel 150 W solar simulator with an AM 1.5G filter. The light intensity was 100 mW $cm^{-2}$. The external quantum efficiency (EQE) measurement was performed under short-circuit conditions with a lock-in amplifier (SR830, Stanford Research System) at a chopping frequency of 280 Hz during illumination with monochromatic light from a Xenon lamp.

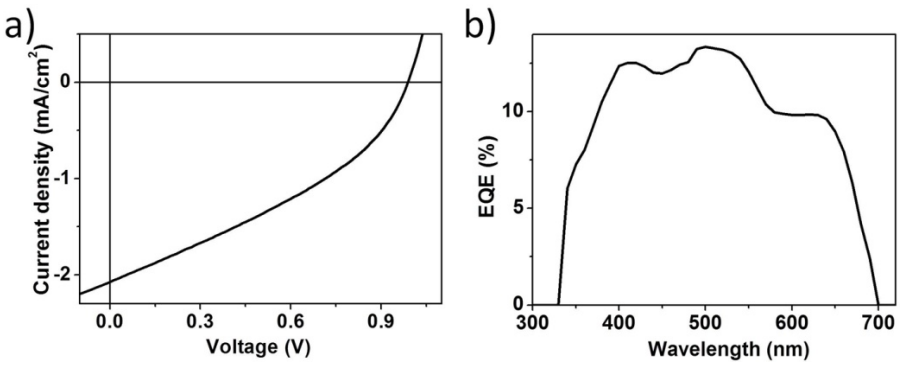


**Figure S11**. a) *J*–*V* curve and b) EQE spectrum of the OSC device processed with 1-butanol.

The OSC device processed with 1-butanol shows a PCE of 0.73%, with a $V_{oc}$ of 0.99 V, a $J_{SC}$ of 2.07 mA $cm^{-2}$ and an FF of 35.6%. The EQE spectrum spans from 330 to 700 nm with a maximum value of 14%. The $J_{SC}$ calculated by integration of the EQE curve is in good accordance with the value obtained from the *J*-*V* measurement.

## 9. Surface morphology of active layer and neat films of BDT and D-OEG

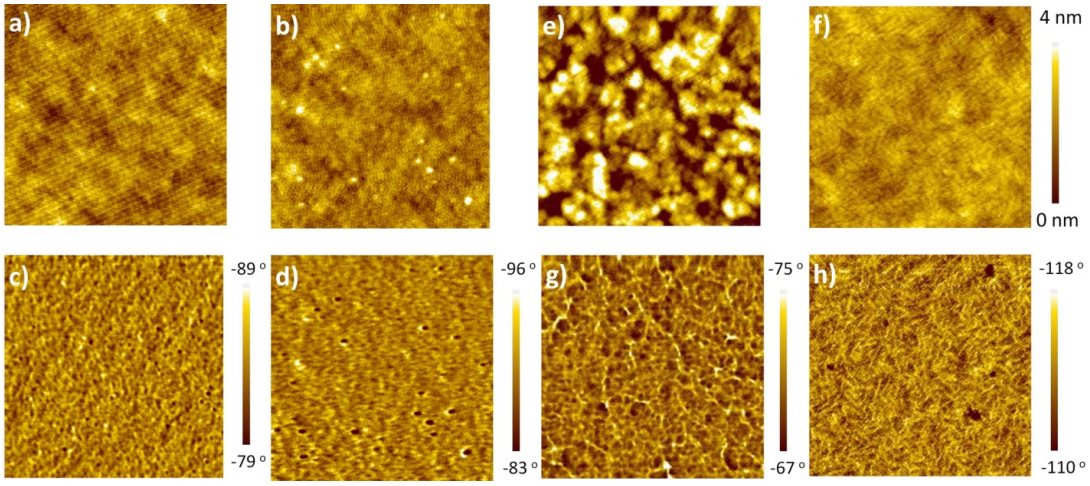


**Figure S12**. AFM height images of active layers processed with a) 1-hexanol and b) 1-butanol; AFM phase images of active layers processed with c) 1-hexanol and d) 1-butanol. AFM height images of neat films of e) **BDT** and f) **D-OEG**; AFM phase images of neat films of g) **BDT** and h) **D-OEG** processed with 1-hexanol. The scale size is 2 μm × 2 μm.

The neat film of **BDT** shows spheroidal aggregates with domain sizes of more than 200 nm; the surface root-mean-square (rms) roughness is calculated to be 2.81 nm, which implies that severe aggregation is occurring. The neat film of **D-OEG** shows a homogeneous morphology with obvious fibrous networks; the surface rms roughness is calculated to be 0.60 nm.

However, for the active layer consisting of **BDT** and **D-OEG** an ordered array of fibers was not observed. A possible reason is that the severe aggregation of **BDT** inhibits the ordering of blends. The amorphous morphology in the active layer is detrimental to the charge carrier transport. Besides, the strong aggregation of **BDT** may lead to local phase separation in the active layer, which likely hampers exciton diffusion and dissociation, leading to the modest $J_{SC}$ and FF.

## 10. Comparison of the optical properties and mobilities of BDT with those of other related semiconductors.

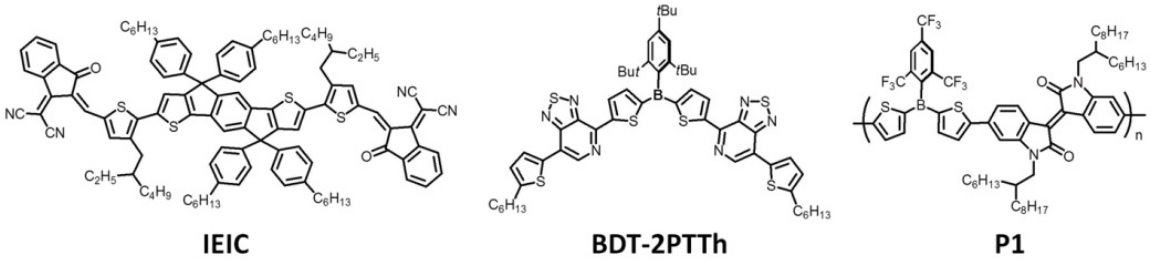


**Figure S13**. Chemical structures of **IEIC**, **BDT-2PTTh** and **P1**.

**Table S4.** Photophysical characteristics and electron mobilities of **BDT**, **IEIC**, **BDT-2PTTh** and **P1**.

| | $\lambda_{max}^{sol}$ (nm) | $\lambda_{max}^{film}$ (nm) | $E_g^{opt}$ (eV) | $\mu_e$ ($cm^2\ V^{-1}\ s^{-1}$) | Ref. |
|---|---|---|---|---|---|
| **BDT** | 477 | 487 | 2.16 | $1.37\times10^{-5}$ | this work |
| **IEIC** | 672 | 722 | 1.57 | $1.60\times10^{-4}$ | [4] |
| **BDT-2PTTh** | 507 | 525 | 2.01 | $6.40\times10^{-5}$ | [5] |
| **P1** | 462/572 | 466/582 | 1.80 | $0.84\times10^{-5}$ | [6] |

The structural skeleton of **BDT** is similar to that of **IEIC**, which is a typical molecular electron acceptor. Both of these compounds have huge steric hindrance at the core unit, and both are end-capped with electron withdrawing groups through thiophene bridges. However, **IEIC** uses a fused donor unit consisting of indaceno[1,2-b:5,6-b']dithiophene as the core, while **BDT** uses a flexible acceptor unit consisting of a triarylborane as the core. As a result, **IEIC** displays a strong low energy absorption with a narrow bandgap of 1.57 eV, while **BDT** absorbs at higher energy with a wider bandgap of 2.16 eV. The mobility of **IEIC** can reach up to $1.6\times10^{-4}$ $cm^{-1}\ V^{-1}\ s^{-1}$, which is higher than that of **BDT**. **BDT-2PTTh** has the same core unit as **BDT**, and both of them are organic semiconductors based on p-π* conjugation with a triarylborane core. **BDT** and **BDT-2PTTh** have similar optical bandgaps which are larger than 2.00 eV. The electron mobility of **BDT** is comparable to that of **BDT-2PTTh**. The conjugated polymer **P1** based on triarylborane units has a medium bandgap of 1.80 eV, a little smaller than that of **BDT**, which may be due to the extended conjugation of **P1**. However, there is little difference in the mobilities between **BDT** and **P1**.

## 11. References


[1] Gaussian 09 (Revision A.02), M. J. Frisch, G. W. Trucks, H. B. Schlegel, G. E.Scuseria, M. A.Robb, J. R. Cheeseman, G. Scalmani, V. Barone, B. Mennucci, G. A.Petersson, H. Nakatsuji, M.Caricato, X. Li, H. P. Hratchian, A. F. Izmaylov, J. Bloino, G. Zheng, J. L. Sonnenberg, M. Hada, M. Ehara, K. Toyota, R. Fukuda, J.Hasegawa, M. Ishida, T. Nakajima, Y. Honda, O. Kitao, H.Nakai, T. Vreven, J. A.Montgomery, Jr., J. E. Peralta, F. Ogliaro, M. Bearpark, J. J. Heyd, E.Brothers, K. N.Kudin, V. N. Staroverov, R. Kobayashi, J. Normand, K. Raghavachari, A. Rendell, J. C. Burant, S. S. Iyengar, J. Tomasi, M. Cossi, N. Rega, J. M. Millam, M. Klene, J. E.Knox, J. B.Cross, V. Bakken, C. Adamo, J. Jaramillo, R. Gomperts, R. E. Stratmann, O. Yazyev, A. J. Austin, R. Cammi, C. Pomelli, J. W. Ochterski, R. L. Martin, K.Morokuma, V. G. Zakrzewski, G. A. Voth, P. Salvador, J. J. Dannenberg, S. Dapprich, A. D. Daniels, Ö. Farkas, J. B. Foresman, J. V. Ortiz, J.Cioslowski, D. J. Fox, *Gaussian, Inc*., Wallingford CT, **2009**.

[2] a) X. D. Yin, J. W. Chen, R. A. Lalancette, T. B. Marder, F. Jäkle, *Angew. Chem. Int. Ed.* 2014, **53**, 9761-9765; b) X. D. Yin, F. Guo, R. A. Lalancette, F. Jäkle, *Macromolecules* 2016, **49**, 537-546.

[3] T. L. Nguyen, C. Lee, H. Kim, Y. Kim, W. Lee, J. H. Oh, B. J. Kim, H. Y. Woo, *Macromolecules* 2017, **50**, 4415-4424.

[4] Y. Z. Lin, Z. G. Zhang, H. T. Bai, J. Y. Wang, Y. H. Yao, Y. F. Li, D. B. Zhu, X. W. Zhan, *Energy Environ. Sci.* 2015, **8**, 610-616.

[5] X. Yin, K. Liu, Y. Ren, R. A. Lalancette, Y.-L. Loo, F. J**ä**kle, *Chem. Sci.* 2017, **8**, 5497-5505.

[6] B. Meng, Y. Ren, J. Liu, F. Jäkle, L. Wang, *Angew. Chem. Int. Ed.* 2018, **57**, 2183-2187.